A machine learning classification of meteorite spectra applied to understanding asteroids

M. Darby Dyar [a,b,*], Sydney M. Wallace [a], Thomas H. Burbine [a,b], Daniel R. Sheldon [c]

[a] Planetary Science Institute, 1700 East Fort Lowell, Suite 106, Tucson, AZ 85719-2395, USA
[b] Department of Astronomy, Mount Holyoke College, 50 College St., South Hadley, MA 01075, USA
[c] College of Information and Computer Sciences | 140 Governors Dr., Amherst, MA 01003, USA

ABSTRACT

Understanding the distribution of matter within our Solar System requires a robust methodology for evaluating the composition of small objects in the asteroid belt. Existing asteroid taxonomies have variously been based on spectral features relating to mineralogy and on classification of asteroid spectra alone. This project tests a fundamentally different approach, using machine learning algorithms to classify asteroids based on spectroscopic characteristics of existing meteorite classes. After evaluating four classification techniques built on labeled meteorite spectral data, logistic regression (LR) was determined to provide the most accurate results that distinguish eight robust groups of meteorite classes to which asteroid spectra can then be matched. The groups are rooted in mineralogical composition and directly relate meteorites to potential host bodies. A standalone LR algorithm classifies unknown asteroid spectra uniquely as one of eight specific group, allowing the distribution of compositions in the asteroid belt to be evaluated.

1. Introduction

We may well be living in the Golden Age of asteroid research (Burbine, 2017). The Dawn mission has mapped the largest and third largest ((1) Ceres and (4) Vesta, respectively) asteroids in the Main Belt and completed geochemical analyses of their surfaces (Russell and Raymond, 2011). The Hayabusa and Hayabusa2 missions have returned asteroid fragments to Earth (Nakamura et al., 2011; Yada et al., 2022), and another asteroid mission (OSIRIS-REx) will land with additional samples (Lauretta et al., 2017). The Lucy mission to a Main Belt asteroid and seven Trojans launched in 2021 (Levinson et al., 2021), and the Psyche mission to a metal asteroid will launch in 2023 (Elkins-Tanton et al., 2020). Public interest in Earth-altering impacts is high as evidenced by news stories and movies, and the potential for mining asteroids has been studied (e.g., Kargel, 1994). The attention is further justified because asteroids represent important building blocks of our Solar System. They hold the keys to furthering our understanding of planet formation and evolution from a dust-filled protoplanetary disk (Burbine, 2017). Although data on asteroid compositions have paramount importance to gaining this knowledge, very little is known about them because there have been so few sample return missions. Asteroid imagery and remote spectroscopy provide only tantalizing glimpses into

their surface and bulk compositions. Improving interpretation of those remote measurements is our best hope for learning about the details of the distribution of solid matter within the asteroid belt.

The first steps toward that capability have come from attempts to classify asteroids using features (e.g., bands and slopes) from spectroscopy, which is fundamentally representative of composition. Several such asteroid taxonomies have been developed, (e.g., Chapman et al., 1975; Tholen, 1984; Bus and Binzel, 2002a), most recently the Bus-DeMeo (BDM) classifier (Bus and Binzel, 2002a, 2002b; DeMeo et al., 2009;), which uses slope scores and principal component analysis of reflectance spectra to group similar objects. However, because there are only subtle distinctions among many classes, the current BDM web tool (http://smass.mit.edu/busdemeoclass.html) is challenging to use. It requires visual inspection to classify many objects (e.g., ~40% of objects; Burbine et al., 2019), so the resultant taxonomy is often quite subjective. Its accuracy is unconstrained.

Other studies (e.g., Oszkiewicz et al., 2014, 2023; Klimczak et al., 2021; Penttilä et al., 2021, 2022; Colazo et al., 2022) have applied a wide variety of machine learning approaches to asteroid classification. Mahlke et al. (2022) and Klimczak et al. (2022) leveraged new sets of observations. Although these and other new asteroid-based classifications show tremendous promise for creating useful groups or clusters,

---

they cannot directly contribute compositional or mineralogical insights into the constituents of those groups because they have no such data upon which to train. Such approaches are considered unsupervised in that the true group structure is unknown.

This paper takes a fundamentally different approach by using meteorite spectra, which do represent ground truth for their unknown asteroid parent bodies, and thus their laboratory spectra can be used to develop and test a new asteroid taxonomy. A meteorite-based classification system benefits from a very robust 45-class taxonomy that is based on mineralogical, petrological, and chemical properties; meteorite spectra can thus be labeled by group. This allows the accuracy of machine learning classification models to be evaluated before being applied to asteroid spectra. This project trains machine learning models on 1422 laboratory meteorite spectra and then applies the results to 605 asteroid spectra to evaluate the distribution of compositions in the asteroid belt.

2. Background

Several asteroid taxonomies based on spectroscopy have been developed over the years since the first asteroid spectra were collected (McCord et al., 1970). Chapman et al. (1975) initiated a system for classification by assigning the "*C*" and "*S*" designations to numerous asteroids to differentiate between lower albedo and weaker absorption band bodies (*C*-types) and higher albedo and stronger absorption band bodies (*S*-types). Objects that did not fit into either class (e.g., (4) Vesta) were given the *U* designation. David Tholen (1984) greatly expanded on this taxonomy using data from the Eight-Color Asteroid Survey (ECAS) that observed asteroids from ~0.3 to ~1.1 μm (Zellner et al., 1985).

Bell (1989) tried to link the Tholen (1984) classes to different degrees of heating. He divided the Tholen (1984) classes into three main super-classes (primitive, metamorphic, and igneous) based on the amount of heating the object may have experienced. Bell (1989) assumed that the *S*-types were primarily igneous objects that experienced significant amounts of melting, which is not the common interpretation of those objects today. Many to most *S*-types are now assumed to have ordinary chondrite mineralogies (e.g., Chapman, 1996; DeMeo et al., 2022).

Richard Binzel and students developed a taxonomy using CCD spectra (~0.4 to ~1.1 μm) of asteroids (Bus and Binzel, 2002a) as part of SMASS II (Small Main-Belt Asteroid Spectroscopic Survey). Bus and Binzel (2002b) found that there was a continuum of spectral properties for most asteroid classes and created a number of subtypes. Using the more extensive near-infrared spectral data subsequently collected by the Binzel group coupled with their CCD spectra, DeMeo et al. (2009) created the modern Bus-DeMeo (BDM) asteroid taxonomy, extending the Tholen (1984) and Bus and Binzel (2002b) taxonomies into the near-infrared.

Beginning with Tholen (1984), these classification systems used the statistical method of principal components analysis (PCA) to transform spectra into low dimensions for exploratory analysis, after which they manually defined classes. PCA is one of the oldest multivariate techniques in statistics (first proposed by Pearson in 1901). It transforms a data set with many correlated variables (like the wavelengths of light in reflectance spectra) into the space of principal components, resulting in new variables that are not linearly correlated. The top several principal components may be used as a low-dimensional summary of the data for visualization and exploration. BDM and related classification systems were created by visually identifying clusters in the space of principal components, and then identifying linear decision rules to separate clusters.

There are several limitations of this early approach. Principal components have no intrinsic meaning and simply capture primary axes of variability in the data. They may relate to "nuisance" sources of variability, e.g., from the measurement process, instead of intrinsic variability. This may be a significant problem for data collected using different telescopes or acquisition parameters. However, PCA was a commonly used methodology at the time the BDM taxonomy was developed. PCA is a linear method, so cannot capture non-linear correlations in the data. Finally, PCA treats each spectrum as an unstructured vector and does not understand the relationship between measurements at different wavelengths; it therefore does not make the best statistical use of the limited data.

The most significant weakness of these asteroid-based taxonomies is that they are empirical mathematical constructions that do not link directly to either mineralogy or chemistry — classes are defined visually using clusters in PCA space and are completely phenomenological. Moreover, they were created using small data sets. BDM was originally established using only 371 spectra that were collected using the same telescope and protocol. Because the BDM method uses no "labeled" samples for which ground truth is available, its error analysis is not robust. Finally, differences among spectral classes are subtle, and it is unclear how they relate to mineralogical differences. The same issues arise with more recently proposed asteroid taxonomies that use machine learning.

In contrast, meteorite taxonomy is firmly grounded in mineralogy and chemistry and has been developed over many decades. The current method of classification involves primarily studying a thin section to determine composition, mineralogy, and texture. There are three major super-groups: chondrites (never melted), achondrites (formed from a melt), and irons (which melted and then differentiated). There are also important subdivisions.

Of course, not all meteorite groups are thought to have formed on separate bodies. For example, almost all members of the howardite, eucrite, and diogenite (HED) groups likely originated on one parent body, thought to be Vesta (e.g., McCord et al., 1970; Larson and Fink, 1975; McSween et al., 2013) due to compositional, isotopic, and spectral similarities. However, some HEDs with "anomalous" oxygen isotopic values are thought to originate on separate parent bodies from Vesta (Scott et al., 2009). The linked acapulcoites and lodranites have similar oxygen isotopic compositions but just differ in grain size (McCoy et al., 1997).

Current methodology for distinguishing among these classes requires careful petrologic study and a lot of work. Although this procedure represents the gold standard in meteorite classification, development of an alternate field method for rapid meteorite classification might be useful for preliminary taxonomy. But most importantly, a spectroscopy-based meteorite classification enables compositional relationships to be drawn between meteorites and their parent bodies, and supports creation of an asteroid taxonomy linked directly to that of meteorites.

3. Materials and methods

An overview of the processes used in this project is given in Fig. 1. The underlying basis for this project is the assumption that the best (albeit imperfect) spectroscopic proxies for asteroid belt objects are the meteorites that originate from them. Accordingly, it was necessary to request, prepare, and acquire spectra of a large number of meteorites to ensure that a representative suite of spectra was available for our classification study. Once those data were obtained, several machine learning techniques for classification were tested, and a penultimate model was used to classify asteroid spectra. Details of these steps follow.

3.1. Data studied

Meteorite spectra were acquired on reflectance data acquired at RELAB at Brown University. Some data were acquired on meteorite spectra from their public archive but several meteorite classes were poorly represented. To remedy this deficiency, we requested and received 116 additional meteorites from the Antarctic and other meteorite collections at Johnson Space Center and the National Museum of Natural History and prepared them by hand crushing and sieving to 45–120 μm particle sizes before spectral acquisition. We note that the
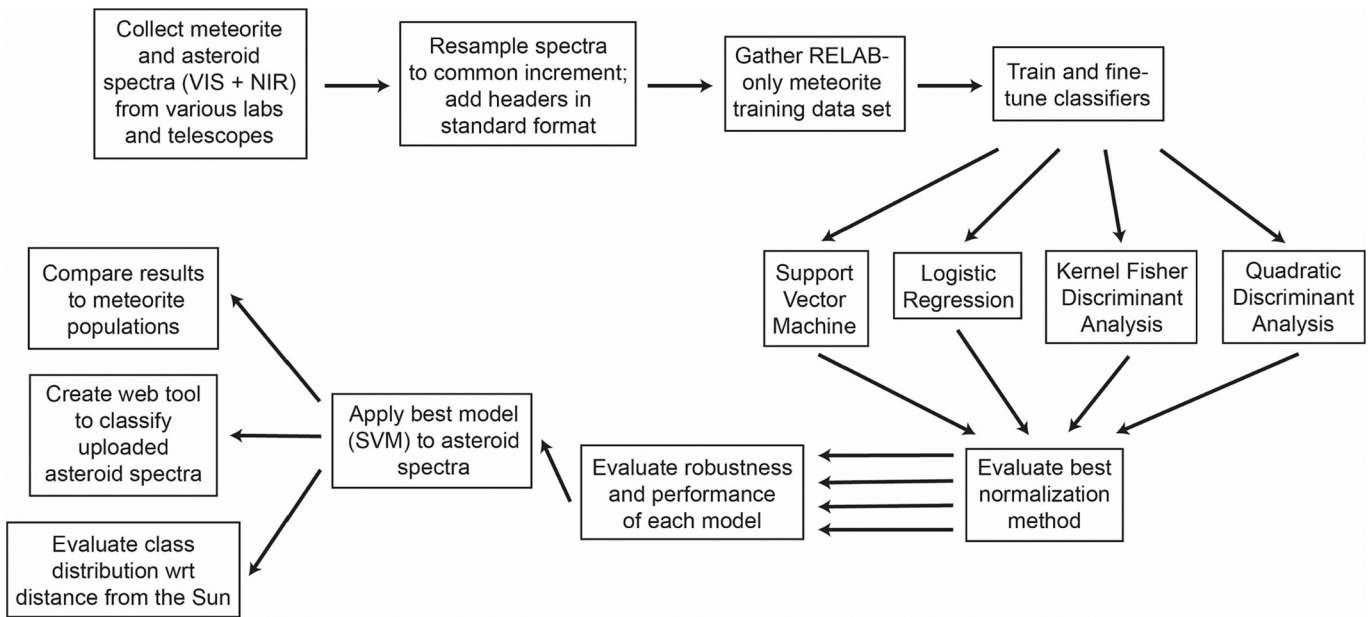
Fig. 1. Flow chart of this project. Steps leading to the three main results.

additional added samples mitigate but do not remove the bias of the RELAB data set toward falls. There is most certainly a mismatch in composition between asteroid populations and the meteorite collections because some asteroid populations are more effective in delivering meteorites to the Earth (Vernazza et al., 2008; Granvik and Brown, 2018; Binzel et al., 2019). Moreover, the meteorite flux is time-

Table 1
Derived classes based on meteorite spectra used to predict asteroid spectra.

Group name	Meteorite class	Major mineral components	Spectral similarity
CM/C2/CR	CM	Fe-Mg serpentines, clumps of tochilinite/cronstedtite, sulfides, magnetite. Chondrules contain olivine, low-Ca clinopyroxene, and isotropic glassy mesostases.	Relatively featureless spectra lacking major olivine and pyroxene features
	C2	Abundant hydrated minerals and abundant fine-grained matrix; chondrules are present; sulfides are Ni-bearing	
	CR	Olivine, low-Ca pyroxene, metallic FeNi, troilite, FeNi sulfides, Fe—Mg serpentines, and magnetite.	
CO/CV	CO	Olivine, low Ca-pyroxene and pigeonite, feldspathic glass, metallic FeNi, and minor sulfides, and CAIs*	Relatively weak absorption features due to olivine and pyroxene
	CV	Olivine, low-Ca pyroxene, glass, metallic FeNi, troilite, anorthite, and CAIs*	
CK/R/ brachinites	CK	Olivine, low-Ca pyroxene, anorthite, diopside, fassaite, magnetite, pentlandite, and CAIs*	Olivine-dominated absorption features
	R	Abundant olivine, less abundant in low-Ca pyroxene. Can also contain pigeonite, augite, diopside, albite or oligoclase, and spinel.	
	Brachinites	Olivine-dominated, Ca-pyroxene, chromite, plagioclase, Fe-sulfides	
H/L/LL/URE	H	olivine, low-Ca pyroxene, pigeonite, FeNi metal, troilite. Approximately equal abundances of olivine and pyroxene. Less Fe-rich olivine and low-Ca pyroxene than L chondrites.	Absorption features due to olivine and pyroxene representing a continuum between varying amounts of olivine and pyroxene
	L	olivine, low-Ca pyroxene, pigeonite, FeNi metal, troilite. Less Fe-rich olivine and low-Ca pyroxene than LL chondrites. Olivine more abundant than pyroxenes. FeNi metal less abundant than H chondrites.	
	LL	olivine, low-Ca pyroxene, pigeonite, FeNi metal, troilite. Olivine much more abundant than pyroxenes. FeNi metal less abundant than L chondrites.	
	Ureilite	Carbon-bearing, olivine-pyroxene achondrites. Typically olivine is more abundant than pyroxene.	
EH/EL/AUB	EH	Low-Ca pyroxene, forsterite, calcic pyroxene, plagioclase, FeNi metal, sulfides	Featureless spectra due to being dominated by enstatite and FeNi metal
	EL	Low-Ca pyroxene, forsterite, calcic pyroxene, plagioclase, FeNi metal, sulfides	
	Aubrites	Enstatite-dominated, albite, diopside, forsterite, sulfides	
ACA/LOD	Acapulcoites	Orthopyroxene, olivine, Cr-diopside, sodic plagioclase, FeNi metal, troilite.	Orthopyroxene-dominated spectra
	Lodranites	Orthopyroxene, olivine, Cr-diopside, sodic plagioclase, FeNi metal, troilite. Coarser grained than acapulcoites.	
IAB/IIAB	IAB	FeNi metal, tetrataenite, troilite, daubréelite, schreibersite	Featureless, slightly red spectra due to the abundance of FeNi and absence of silicates
	IIAB	FeNi metal, kamacite, martensite, taenite, tetrataenite, troilite, daubréelite, schreibersite, cohenite, haxonite, edscottite, graphite, diamond, carlsbergite, chromite, fusion-crust magnetite, merrillite, chlorapatite	
EUC/DIO/ HOW	Eucrites	Igneous volcanic monomict rocks rich in pyroxene (pigeonite) and calcic plagioclase	Continuous range of absorption features due to varying amounts of pyroxene
	Diogenites	Orthopyroxenite monomict rocks with <10% plagioclase and minor chromite, olivine, silica, pigeonite, and augite.	
	Howardites	Polymict breccias composed predominantly of eucritic and diogenitic clasts.	

dependent. Accordingly, this study is only a start at trying to create a representative training set to test the methodology proposed; a logical next step would be to create artificial mixtures of materials and acquire their spectra to try to mimic asteroids believed to be poorly represented in meteorite collections.

The choice to use data from particulate samples was purposeful to avoid effects of variable angles of incidence by presenting randomly oriented grains to the spectrometer. This is likely the best proxy for asteroid spectra, which generally sample a large surface area on an object.

Each of these meteorite spectra was examined for irregularities and removed if the sample appeared to be excessively weathered or the spectra was taken under special experimental conditions. Spectra from class were divided into five different folds such that no two folds contained a spectrum from the same meteorite. If a meteorite class had fewer than five spectra, it was removed from the data set. The only exception to this is that the IAB and IIAB (Table 1) classes were combined and then placed into five folds together. This process culminated in 1422 meteorite spectra spanning 20 classes (Excel table **Data S1**). The remaining classes are unrepresented in this classification but they represent either very rare classes or ones from which it was difficult to prepare particulate samples (i.e., iron meteorites). The meteorite data covered the standard visible to near-infrared range for RELAB, which is from 0.3 to 2.6 μm at increments of either 0.005 or 0.01 μm.

To test the accuracy of the RELAB-based meteorite classification, we obtained a suite of 354 meteorite spectra acquired in the laboratory of Dr. Edward Cloutis at the University of Winnipeg (Excel table **Data S2**). Those data were collected from 0.35 to 2.5 μm at 0.001 μm intervals. Although this data set did not include any representation from the acapulcoite/lodranite class, it does provide a useful test of prediction accuracy for unseen data.

Asteroid spectra were obtained from SMASS (DeMeo et al., 2009) and MITHNEOS (MIT-Hawaii Near-Earth Object Spectroscopic Survey) (Binzel et al., 2019). MITHNEOS includes both NEAs (near-Earth asteroids) and Mars-crossers. The asteroid spectra are primarily a combination of visible CCD (charge-coupled device) spectra and near-infrared spectra taken at the NASA IRTF (Infrared Telescope Facility). The SMASS data range from 0.45 to 2.45 μm at increments of 0.005 μm. The MITHNEOS data, which were taken from a variety of sources, primarily range from ~0.4 to ~2.45 μm at increments of ~0.005 μm. Because many asteroid spectra were unclassified, Burbine et al. (2019) determined and cross-checked Bus-DeMeo classes for 605 asteroid spectra using either the supplied labels from MIT or the online tool. A list of spectra analyzed is given in Excel table **Data S3**.

Meteorite and asteroid data were compressed by downsampling using 'decimation' to cover the range from 0.35 or 0.45 (i.e., beginning at the lowest wavelength of the source spectra) to 2.5 μm at 0.01 μm resolution. Every nth data point was used, depending on the resolution of the source spectra as given above.

Spectral data files were reformatted for consistency with attached headers containing acquisition parameters and other information. The same set of headers was used for both meteorite and asteroid data for ease of manipulation.

Existing data were split into different groups for training and evaluating a machine learning classifier. The large meteorite and asteroid data sets were each separated into three groups: *training data* (60% of spectra) to build the models, *validation data* (20%) to choose which model had the best performance, and *test data* (20%) to evaluate the accuracy of the best-performing model. Selection of spectra for each group was stratified such that the number of spectra from the same group represented in each dataset reflect these same proportions.

3.2. Data analysis tools

Data analysis used an in-house tool written by Sydney Wallace in Python and utilizing the SciKit-learn library as described in Carey et al.

(2017). Data pre-processing techniques were evaluated for their potential to standardize spectra and improve classification performance. It was hoped that they might transform the data in each class to be more consistent and exacerbate differences among other classes. For logistic regression (LR), baseline removal (BLR) was tested using Fully Automated Baseline Correction (FABC) (Cobas et al., 2006; Kajfosz and Kwiatek, 1987), Adaptive Iteratively Reweighted Penalized Least Squares (AirPLS) (Zhang et al., 2010), Asymmetric Least Squares (ALS) (Eilers and Boelens, 2005), or Morphologically Weighted Penalized Least Squares (MPLS) (Li et al., 2013). These were found to improve prediction accuracy only slightly, from ~55% for no BLR to ~60% for an LR model. Support vector machine (SVM) models are more accurate (~63%) and relatively insensitive to pre-processing; this is likely due to the fact that they learn non-linear models and have capacity to automatically cope with the types of variation (scaling, offset, linear trend, etc.) that pre-processing seeks to control. Normalization, squashing, and smoothing also affect accuracy in different ways depending on which baseline removal algorithm is used. In general, we found that while some methods create greater similarity within classes, they also remove information embedded in the data that would benefit classifiers. For this reason, we only used only one preprocessing method, which was normalization.

Normalization is necessary allow data acquired for different durations and under varying conditions to be compared, not only for the meteorite models but also to allow predictions of asteroid belt objects based on their spectra. The philosophy behind normalization for spectral data is to try to find the wavelength that is most invariant and therefore relatively constant in all the spectra analyzed. In this application, spectra over the VNIR are affected to first order by the composition of the meteorites/asteroids being studied. For example, varying amounts of pyroxene and olivine will affect intensities around 1 and 2 μm, so those wavelengths would not be optimal for normalization. Other factors affecting spectral intensity include many of the steps in the pipeline by which spectra images are reduced. These include factors such as flat field correction, sky subtraction, wavelength correction and atmospheric correction (Binzel et al., 2019). Because of all the factors affecting spectral intensity at varying wavelengths, it is perhaps unrealistic to expect any "idea;" wavelength for normalization.

Normalizing the spectral intensity at 0.55 μm, which is the solar maximum and center of the V filter band, is a common but untested historical convention (e.g., Bus and Binzel, 2002a, 2002b; Penttilä et al., 2021); others have used the center of the J filer band at 1.215 μm (e.g., Binzel et al., 2019). Given this potential ambiguity, the optimal wavelength for classification in our data set was evaluated by normalizing all meteorite spectra to every wavelength between 0.35 and 2.5 at 0.05 μm increments to look for optimal performance (**Fig. S2**) for all four classifiers. The most accurate wavelength for each model was used in subsequent asteroid predictions as seen in Fig. 2. The LR model normalized to the energy at 0.70 μm was ultimately chosen as the optimal model for application to asteroids, albeit with incremental improvement over the choice of 0.55 μm.

3.3. Experimental design

Four different classifiers were considered for this task: LR, SVMs, kernel fisher discriminant analysis (KFDA), and quadratic discriminant analysis (QDA). Background on the SVM, LR, and QDA methods is given in Hastie et al. (2009) while KFDA is discussed in Mika et al. (2001). LR, SVM, and KFDA are discriminative models, which means they are optimized to discriminate samples of different classes as opposed to modeling the full distribution of all samples within each class. All methods can also be characterized by the type of decision boundaries within the data space they use to classify samples. LR uses linear decision boundaries, QDA uses quadratic boundaries, and kernelized SVM and KFDA both allow the boundaries to be non-linear in a way that depends on the kernel.
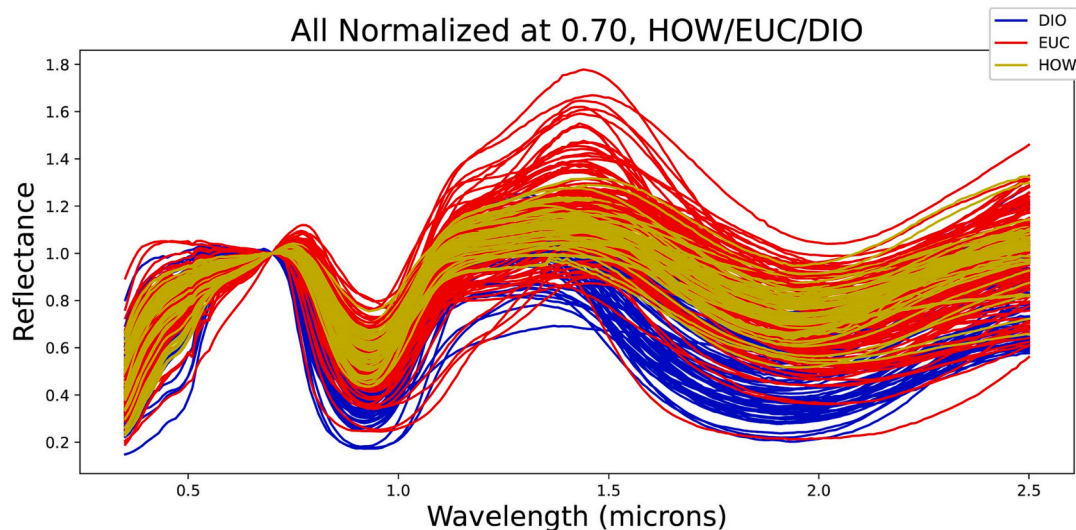
Fig. 2. Spectral similarity within a sample class. VNIR spectra of HOW/EUC/DIO meteorites from the RELAB training set data, normalized to 0.70 μm. All the spectra have the same general shape, resulting from variable amounts of pyroxene group minerals, which have bands ca. 1 and 2 μm.

Logistic regression predicts the probability that a sample belongs to each class given a set of features and parameters. It first assigns a real-valued score to each class, then uses a "softmax" function to map class scores to probabilities, which are nonnegative and sum to one. The class scores are linear functions of the features with parameters or "weights" to be learned by numerically maximizing the log-probability of the correct class averaged over all training examples–i.e., the conditional log-likelihood (given the features). There are many algorithms for conducting the maximization, but LBFGS was chosen because it is commonly used with mid-size and small datasets. The number of iterations for training was limited to 1500. To keep the model from overfitting, an L2 regularization hyperparameter was included to penalize larger weights. However, results showed that not much regularization was needed to achieve optimal performance. The best regularization value found for our dataset was 218.

An SVM is different from LR in that instead of trying to maximize the likelihood, it attempts to place decision boundaries to create the largest margins between classes. Furthermore, a kernel function can be employed to make a kernel SVM, which nonlinearly maps the data from the input space to a higher dimensional feature space. Kernel SVMs use linear decision boundaries in the higher-dimensional feature space, which correspond to non-linear boundaries in the original space. Therefore, kernelization can be thought of as turning a linear model into a nonlinear model and providing greater model flexibility. The trick to doing this without drastically higher computational costs is to represent the data via the kernel matrix giving the pairwise similarity comparisons between the data. The RBF kernel was chosen as it is the most widely used kernel and is known to handle most types of data considerably well. The hyperparameters for this model are the regularization constant (C) and kernel inverse length-scale gamma. Again, a larger C value was used which allows more flexibility for the decision surface. Gamma controls how much influence a given sample has over those around it. A larger gamma value will cause a given training example to only have influence on data that are closer to it. The optimal model had a C value of 218 and a gamma of 0.00045.

KFDA is a kernelized version of linear discriminant analysis. KFDA attempts to project each instance of data into a subspace that maximizes the variance between class means and minimizes the variance between data within the same class. These two optimization problems can be merged via a function known as the Fisher criterion (*29,30*). The solutions to the optimization problems are known as Fisher directions, and they divide the classes based on where the data from different classes differ and where the data within a class are close together. Again, the

RBF kernel was selected and the model was set to find eight Fisher directions, the maximum number of directions allowed for the eight defined classes in this taxonomy. Model performance when trained with eight Fisher directions performed far better than models trained with fewer Fisher directions. Again, gamma was another hyperparameter since the RBF kernel was used. The model with a gamma value of 0.0004 achieved the best validation performance.

QDA was the only true generative model implemented in this study in that it constructs a class conditional probability distribution for the samples within each class, rather than just drawing decision boundaries between classes. It performs supervised dimensionality reduction by projecting the data into a linear subspace that maximizes class separation. Given the class-conditional distributions, Bayes' rule is used to calculate the conditional probability (i.e., posterior probability) of the class label given the sample, for each possible label. The class that maximizes the posterior probability is then selected as the prediction for that sample. QDA assumes that the data is normally distributed within classes. It does not require each class-conditional distribution to share the same covariance, but instead uses a user-defined regularization parameter to penalize the per-class variance. This is what allows QDA to have greater complexity than linear discriminant analysis: if all class-conditional distributions shared the same covariance, the resulting decision boundaries would be linear. Prior to training the QDA model, principal component analysis (PCA) was used to transform the training data into eight components to then be fed as input for QDA. This helped QDA handle collinearity better within the data and improved model performance.

There are different hyperparameters to tune to achieve the best model version possible for any ML task. It is typical to select hyperparameters by measuring the performance on held out data. Cross-validation is a hold-out scheme that makes efficient use of the training data, which is imperative for training models on smaller datasets such as this one. For hyperparameter tuning, we searched exhaustively over a grid of hyperparameter values for each type of model to find the best combination. We used a train/validation/test cross-validation scheme that allows both model selection and estimation of generalization performance. Specifically, the data were split into five folds with three folds always used for training, one fold for validation, and one fold for testing. For each of the 20 distinct ways to split the folds into train, validation, and test sets, and each hyperparameter setting, the model was trained on the train folds and evaluated on the validation fold, resulting in 20 validations scores. These scores are averaged to assign an overall score, and then compared against all other versions of the model to decide on

the best hyperparameters.

Once the top hyperparameter values were selected for each model, an overall score was calculated for each model using the test folds. Several evaluation metrics could have been used here, such as balanced accuracy or F1 score, to deal better with problems involving unbalanced datasets. Although those might be pursued in our future work, for the current project we chose to follow the principle of Occam's razor. Thus, the metric used was simply the percentage of accurate predictions by the model, either for the cross-validated data (internal accuracy of the model predicting other spectra in the same model – i.e., "seen" data) or test or validation data, which are unseen by the model during training. To express this in equation form:

$$model\ accuracy = \frac{\#correct\ predictions}{\#total\ predictions}.$$

For each of the five possible test folds, the model was trained on the remaining four folds using the best hyperparameters from the cross-validation procedure, and then model accuracy was evaluated using the test fold and assigned a test set score.

At the end, the average of the five test scores were calculated and treated as the test score for that model. The confusion matrices seen in the results section of this paper show the predictions for all of the samples from the combined test folds, where, for each sample the prediction is made using the model trained on the four other folds.

4. Results

4.1. Meteorite classification on the basis of spectroscopy

The existing, venerable meteorite classification system is based on a combination of mineralogy, grain size, and texture. In contrast, the proposed meteorite/asteroid classification is based on spectroscopy, which may only be partially sensitive to these variables. To a large extent, features in the 0.35–2.5 μm wavelength region arise from crystal field transitions between oxygen, iron, and other transition metals, though the positions of the bands vary with mineralogy. Grain size generally affects peak intensity rather than position. Thus composition has the biggest influence on spectral properties, with mineralogy also being important and effects of grain size being second order. As a result, meteorite classes with identical mineralogies but difference grains sizes may be spectrally difficult to distinguish on the basis of shape alone because they have all the same peaks, albeit with possibly different intensities as a function of abundance. Classes distinguished only by textural variations will also be spectrally inseparable.

Therefore, it was necessary to group some of the 20 meteorite classes before building a robust classifier. Groups were created using knowledge about the mineralogy and petrology of each meteorite class as well as inspection of the data (e.g., Table 1). Similar mineralogies were grouped together, as were spectra with similar appearance (Fig. 2 and Fig. S1). For example, the parent body for all three classes of HED (howardite-eucrite-diogenite) meteorites is believed to be the asteroid (4) Vesta, which is differentiated and has a basaltic crust from which these classes were sampled. All three groups contain varying amounts of plagioclase feldspar and Fe-rich pyroxenes. Reflectance spectra arising from Fe in the pyroxenes gives rise to characteristic bands at 1 and 2 μm, but the intensities and wavelength of those absorptions vary with the amounts and types of pyroxenes present (Fig. 2). The overall shape of the spectra is similar, and distinctive enough to be easily recognizable by the ML algorithms. Spectra of the other groups, provided in **Fig. S1** and **Data S1,** all display similarly unique signatures in each group. Meteorite class groupings, their characteristics, and the resultant eight combined groups are given in Table 1.

Using the eight groups and 1422 meteorite spectra from the Reflectance Experiment Laboratory at Brown University (RELAB), four classification algorithms were then compared: KFDA, LR, QDA, and SVM as above. Models were trained on 60% of the data and validated using

cross-validation on 20% of the data; the remaining 20% were used for test data. Classification accuracies on validation data using those four models were 92.0%, 90.1%, 88.4%, and 92.0, respectively (Fig. 3).

4.2. Robustness of meteorite classification

Because the classification will be applied to a completely different type of data (i.e., from asteroids), it is desirable to test the putative meteorite classifier on unknown data. For this purpose, we used a suite of 606 meteorite spectra collected in the laboratory of Dr. Edward Cloutis at the University of Winnipeg (**Data S2**). All four algorithms were used to predict those data, with accuracies of 91.2% for KFDA, 91.8% for LR, 85.3% for QDA, and 90.4% for SVM (Fig. 4). So even though the training and test data here come from completely different instruments and analytical conditions, the meteorite groups can still be predicted with >85% accuracy. This result lends confidence to the capability of the RELAB-based model to predict spectral data from other sources such as those from asteroids. By comparing Winnipeg sample results with those from validation on the RELAB set, it was concluded that the LR models generally performed the best overall, and should thus be used as a standard for asteroid prediction. However, we continued to test SVM and KFDA models to see if there would be variations when they were used to predict asteroids.

4.3. Prediction of asteroids into groups based on meteorites

Models built using the top three classification models (SVM, LR, and KFDA) were applied to the asteroid data set and the percentages of asteroids in each of the eight categories were calculated. To put the results in context, they can be compared to meteorite populations. Meteorite falls reported in the Meteoritical Bulletin were tabulated for each category of meteorites used in this study (as of July 2021), representing 64,647 meteorites. Relative percentages in each of our eight groups were calculated. The distribution among types is qualitatively similar to the meteorite classes represented in our RELAB-based training set data (Fig. 5). For example, the largest percentage of falls is classified as L/H/LL/URE and that is also the largest class in the asteroids.

If meteorites were to represent the distribution of different types of material in the asteroid belt, then meteorite abundances in each of our eight meteorite groups should roughly match the distribution of asteroid types predicted by our classification models (SVM, LR, and KFDA). Fig. 5 shows that this is a good approximation despite differences between the populations of meteorites delivered to Earth and the near-Earth and Main belt populations of asteroids, as well as their effectiveness in delivering material to Earth. There is no reason to expect a direct correspondence between the asteroid distribution results and the constituency of the falls or the RELAB data sets; in many cases, the latter either over- or under-represents a class. Thus the numbers of samples in our training sets do not appear to be biasing the classification outcomes. However, the major conclusion from these results is that the L/H/LL/URE group is by far the most abundant in all three asteroid prediction models and in falls and RELAB data as well.

A simple html file to classify an unknown asteroid is available from the authors.

5. Discussion

5.1. Choice of model

Because the asteroid data are unlabeled (i.e., the true composition is largely unknown) and the test results are fairly comparable, there is no obvious criterion for choosing the final model for assigning asteroid data to one of our eight groups. However, the Excel sheet **Data S3** shows that the different algorithms do produce subtly variable predictions, which is unsurprising because all the tested classifiers are distinct.

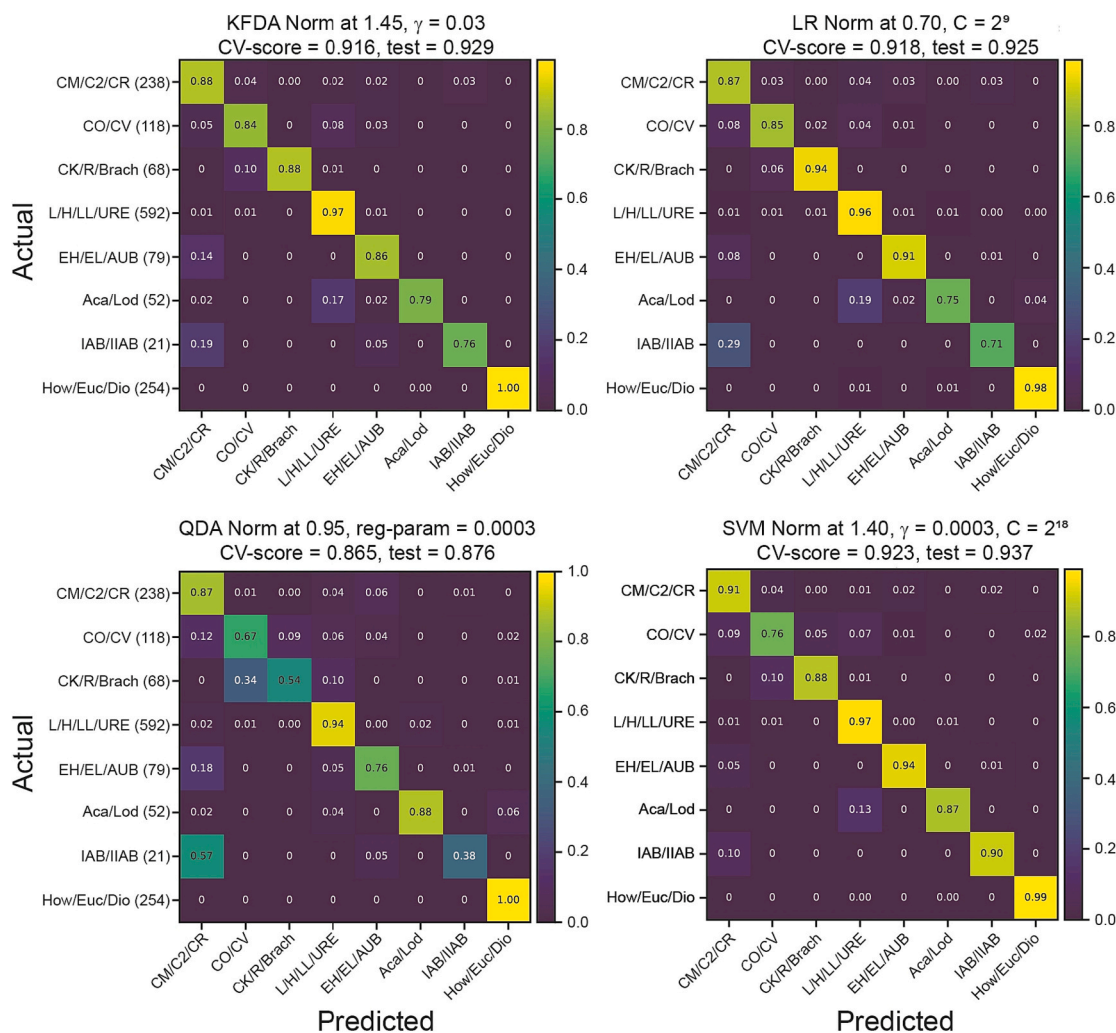The preferred model was therefore chosen by use of consensus

Fig. 3. Validation set accuracy for RELAB meteorite spectra. Confusion matrix showing accuracy of the meteorite classifiers for each of the four techniques tested using the optimal wavelength for normalization of each. The left side labels are the eight different meteorite groups, each with its own distinct spectral signatures. The bottom row indicates the groups to which each spectrum was assigned by the model. A value of 1.0 indicates a perfect match between the model and reality, while a zero value indicates complete mismatch. All models perform comparably except QDA, which has slightly poorer test accuracy.

(Fig. 6) by comparing predictions from KFDA normalized at 1.45 μm, SVM at 1.40 μm, LR at 0.70 μm, and QDA at 0.95 μm. Of the 605 asteroids classified, 315 asteroids were classified identically by all four methods, 157 had one outlier, 121 had two identical groups, and 12 asteroids were classified differently by all four models. In all, there were 29 objects with a unique (i.e., outlier) LR classification, 147 for QDA, 52 for SVM, and 157 for KFDA (values under Y labels in Fig. 5), so the LR classification represented consensus most frequently, and thus was chosen as the final classification.

Objects that were harder for the models to predict resulted in all models producing different results or a split opinion. However, such objects were generally asteroids for which it is believed that there are no representatives in the terrestrial meteorite classes. This is an acknowledged weakness of the method used in this study, for which there can be no remedy until additional meteorites can be measured. Moreover, many of the asteroids with multiple classifications do not have coverage of the range used by our algorithms, which likely confounds definitive classifications.

5.2. Robustness of asteroid classification

Because this study creates an asteroid classification using labeled meteorite data, model accuracy is well-constrained. However, model robustness can also be assessed using two lines of thought: independent knowledge of asteroids and comparison to the existing Bus system. Table 2 compares the presumed meteorite class (see references below), the Bus-DeMeo class, and classifications based on the four models developed in this study. Asteroid (6) Hebe, which was not used in the training or test data, is also predicted for this table. It is apparent that each of the ML models has a very different process for arriving at a given classification but that there is remarkable concurrence.

In most cases seen in Table 2, the models are unanimous is predicting an appropriate composition based on other knowledge of those objects. All of the models agree that Vesta has an HED surface, which is independently known on the basis of Dawn observations (McSween et al., 2013). Angelina, Hungaria, and Eger have been proposed to be similar to enstatite-dominated aubrites (e.g., Clark et al., 2004) because of their extremely high albedos and an absorption band shortwards of 0.55 μm that is characteristic of oldhamite. These three objects are similar to enstatite chondrites, which have much lower albedos than aubrites but similar spectral shapes. Fortuna has an absorption feature at 0.7 μm that is characteristic of CM2 chondrites (Burbine, 1998). Itokawa is known to have an LL chondrite surface, also due to analyses of the returned sample (Nakamura et al., 2011). Apophis has an interpreted composition from its absorption bands similar to LL chondrites (Reddy et al., 2018).

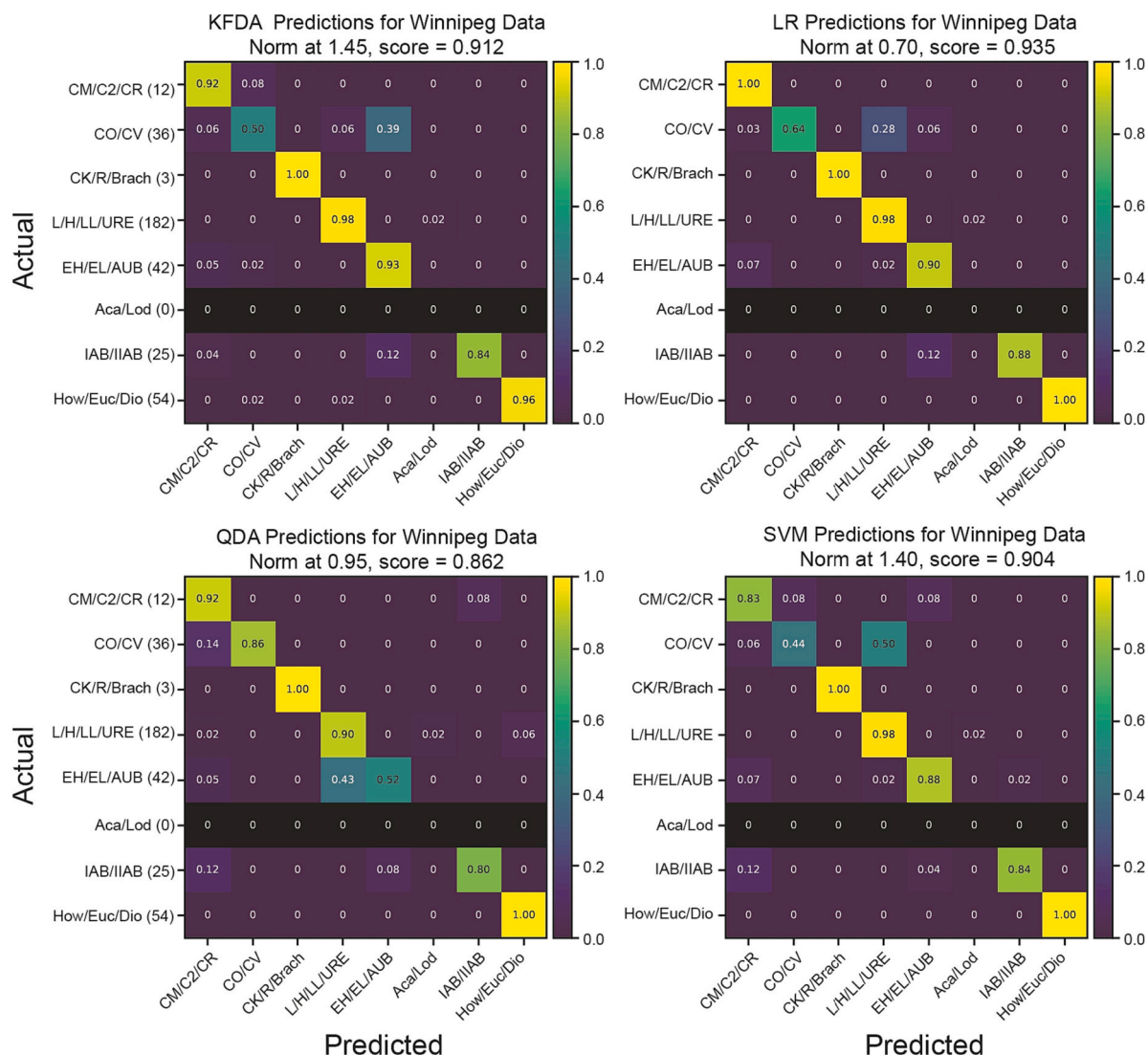For two of the objects where there are no returned samples, our

Fig. 4. Test accuracy of proposed classification. Confusion matrix showing prediction accuracy from application of the RELAB meteorite spectral models to prediction of meteorite class using data from a different instrument at the University of Winnipeg. There were no acapulcoites or lodranites in the Winnipeg data.

results lend insights into speculations about their surfaces. Psyche was once thought to have an iron-dominated composition due to its relatively featureless spectrum and its high radar albedo (e.g., Matter et al., 2013), but recent work acknowledges that meteoritic analogs might span a range from iron meteorites to pallasites, mesosiderites, CB chondrites, and enstatite chondrites (Elkins-Tanton et al., 2020). For Psyche, our classifiers are also somewhat equivocal, but the suggested meteorite groups are also similar. The composition of Hebe has been interpreted from its absorption bands to be similar to H chondrites and IIE iron meteorites (Gaffey and Gilbert, 1998), as predicted by our LR and KFDA models, respectively.

These data from Hebe affirm the choice of LR as the preferred classifier from among the four models tested. LR gives reasonable and believable results for all the objects for which independent information is available. It is striking that the new meteorite-based algorithm does correspond roughly to the Bus-DeMeo system (**Table S3**). For example, a majority of the Q types in the Bus-DeMeo system are L/H/LL/URE in the new classification, as are all but a handful of the S class asteroids. These results make sense because these meteorites all are composed of mixtures of olivine and pyroxene plus opaques. Moreover, all but one of the 27 Bus-DeMeo V asteroids are classed with HED's, and 18 of the 21 D types are grouped with IAB/IIAB/D.

A key difference between our approach and those of others is the use of labeled rather than unlabeled data. Labeled data provide the advantage of classification with known uncertainty, while unlabeled data are very difficult to ground-truth. Prior classifiers using unlabeled asteroid data use varied techniques for classification. For example, the venerable Bus-DeMeo taxonomy primarily classifies objects on the presence or absence of absorption bands and the shape and strength of the bands. The Bus-DeMeo taxonomy groups objects into (currently) 25 different asteroid classes, which is far larger than the eight classes developed here. However, use of the Bus-DeMeo classification frequently requires naked eye assessments, and thus may produce different answers based on the user. The DeMeo and Carry (2014) compositional mapping of the asteroid belt grouped objects into only 12 separate classes due to grouping subtypes (e.g., Cb, Ch, Sq, Sr) into their primary asteroid class, which recognizes that the Bus-DeMeo taxonomy is not grouping all bodies just according to mineralogy. For example, particle size can potentially affect an object's Bus-DeMeo classification by reddening the spectrum or changing the strengths of absorption bands.

Several other recent papers have developed matching algorithms and used machine learning methods for classification of asteroids using the growing libraries of asteroid spectra. Popescu et al. (2012) created a tool using principal component analysis and G-mode clustering to compare
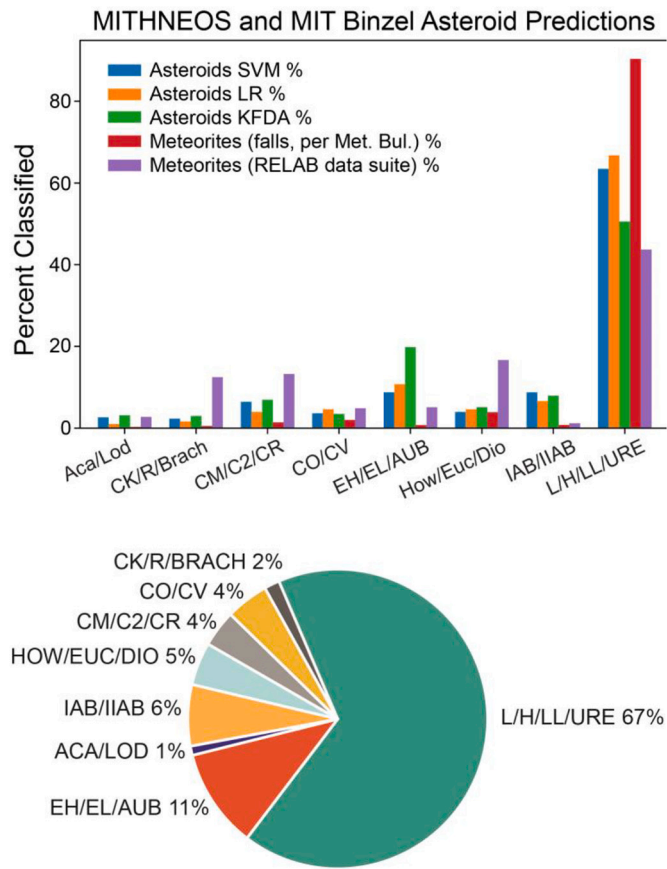
Fig. 5. Classification of asteroids and meteorites. Distribution of asteroid classes using the classifier trained on meteorites. (top) Sample distribution among the eight meteorite-based spectral classes as predicted by SVM, LR, and KFDA models compared against the population of meteorite types in falls and in our RELAB-based training set data. (bottom) Pie chart of percentages of asteroids in each of the eight classes from the LR model.

spectral libraries with asteroid spectra. Oszkiewicz et al. (2014) used a Bayes Naïve Classifier to search for V-type objects, ackowledging that their method will benefit from a larger data set. Their recent paper Oszkiewicz et al. (2023) identified basaltic asteroids observed by the Gaia space mission to used gradient boosting, support vector machines and multilayer perceptrons. Klimczak et al. (2021) has recently broadened their approach to include logistic regression (see also Klimczak et al., 2022). Penttilä et al. (2021, 2022) apply artificial neural networks and deep learning techniques to asteroid classification, linking their results to the Bus-DeMeo classification as we have done in this paper. Colazo et al. (2022) used the clustering tool called fuzzy C-means to propose a zero-phase angle asteroid taxonomy. Mahlke et al. (2022) uses a common factor analyzers model to build a cluster-based taxonomy from spectrometrey and albedo. These studies represent examples of the many machine-learning approaches being applied with enthusiasm to the task of asteroid taxonomy, enabled by the rapid growth of observational databases for asteroids. At some point, it will be useful to combine these unlabeled approaches to the labeled ones to allow compositional and mineralogical information to be better related to proposed unlabeled classes.

5.3. Limitations and considerations

The approach used in this study has limitations associated with both the meteorite data used and the asteroid data. For the former, the constitution of the RELAB data set used for training and potential modification of meteorites by shock must be considered. For the latter, many of the systematic effects are described in detail by Binzel et al. (2019), and need only be discussed briefly here.

5.3.1. Dependence of models on training data

Prior classification studies linking asteroids to meteorites using spectra are based on limited data (e.g., Korda et al., 2023); our study required nearly a decade as we identified gaps in the existing meteorite spectral libraries, requested samples to fill them, and then prepared them for spectroscopy and ran them. However, we recognize that the constitution of our training set is a key limitation of this project, just as it is a limitation of most any machine learning method. It is hoped that subsequent workers will continue to expand the library of meteorite spectra as new meteorites are discovered to grow the potential training
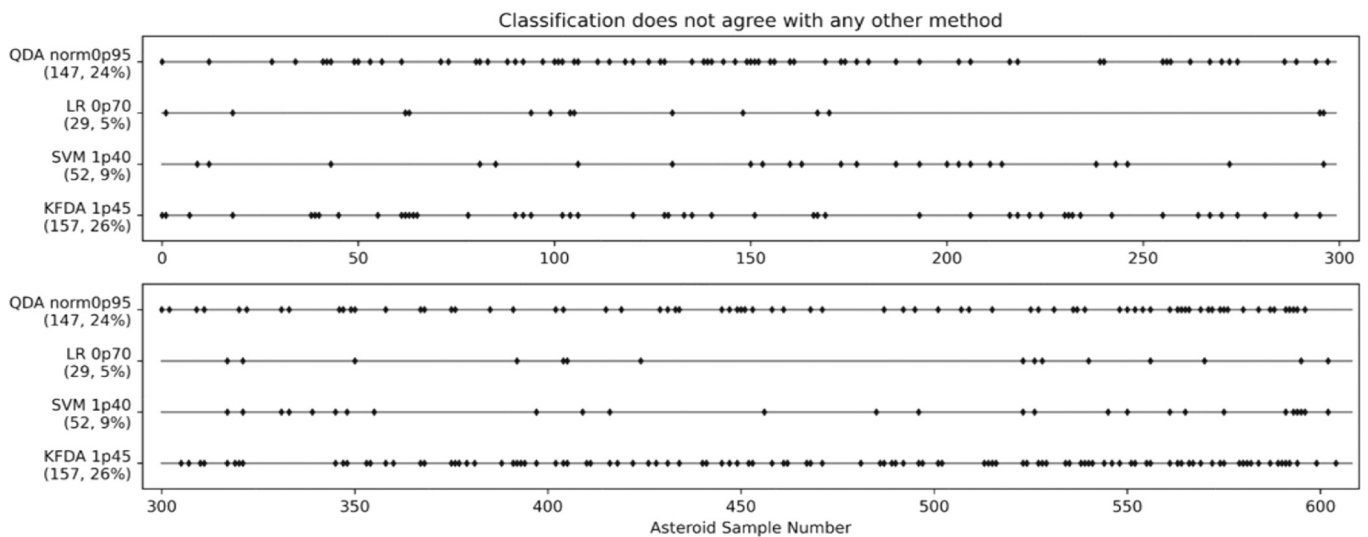

Fig. 6. Consensus plot for asteroid data. Samples numbers are arbitrary, but represent the 605 asteroid spectra studied. Diamonds on each line represent the asteroids for which the given classification results do not match those of a majority of the other objects. Because there are only 29 objects with a unique (e.g., outlier) LR classification versus 147 for QDA, 52 for SVM, and 157 for KFDA, the LR model is chosen as the most generally applicable algorithm to use for identifying asteroid class.

Table 2

Comparison of known or presumed asteroid types with Bus-DeMeo classes and predictions from the four ML models in this study.

Object	Known/ presumed	BDM	SVM	QDA	LR	KFDA
(4) Vesta	HED	V	HED	HED	HED	HED
(3103) Eger	Aubrite	Xe	EH/EL/AUB	EH/EL/AUB	H/EL/AUB	H/EL/AUB
(64) Angelina	Aubrite	Xe	EH/EL/AUB	EH/EL/AUB	EH/EL/AUB	EH/EL/AUB
(434) Hungaria	Aubrite	Xe	EH/EL/AUB	CM/C2/CR	EH/EL/AUB	EH/EL/AUB
(19) Fortuna	CM2	Ch	CM/C2/CR	CM/C2/CR	CM/C2/CR	CM/C2/CR
(25143) Itokawa	LL	Sq	L/H/LL/URE	L/H/LL/URE	L/H/LL/URE	L/H/LL/URE
(99942) Apophis	LL	Sq	L/H/LL/URE	L/H/LL/URE	L/H/LL/URE	L/H/LL/URE
(16) Psyche	EH/EL-CH/CB-IAB/IIAB	Xk	IAB/IIAB	CM/C2/CR	EH/EL/AUB	EH/EL/AUB
(6) Hebe	H	S	ACA/LOD	HOW/EUC/DIO	L/H/LL/URE	IAB/IIAB

set and avoid the bias inherent in existing data.

It is also apparent that some asteroids classes may not be represented in meteorite collections; for example, "exact" carbonaceous chondritic analogs for B-types have been difficult to determine (e.g., Clark et al., 2010). However, it is possible that with dedicated effort, mechanical mixtures of minerals could be created to mimic rare meteorite types that are lacking or poorly represented in existing meteorite collections and thus in spectral libraries. As an example of this approach, Korda et al. (2023) mined mineral mixtures from RELAB (many of which were created by our group) and other databases to develop their mineral-based classification. The accessibility of new natural and mixture-based analog meteorite spectra and future additions to such databases should boost the development of new approaches leveraging them, providing an alternative to classifications using only unlabeled asteroid data (see below). Our goal here is not to present a penultimate meteorite-based classification, but rather to lay the groundwork for additional work using our approach as new data become available.

5.3.2. Shocked phases in meteorites

A related issue deals with the potential effects of shock and impact processes on our meteorites and, consequently, on their spectra. Effects of shock on meteorites and their mineral constituents are well-understood (Bischoff and Stöffler, 1992) and their spectral signatures have been well-studied (Adams et al., 1979; Bruckenthal and Pieters, 1984; Johnson and Hörz, 2003; Treiman et al., 2007; Roberts et al., 2019). For example, it is well-established that plagioclase is the first mineral phase to be affected by shock (becoming maskelynite); however, it has little influence on VNIR spectra due to its low iron content. Kohout et al. (2020) conducted experiments on a sample of the Chelyabinsk LL5 meteorite and found shock darkening due to the formation of fine troilite-metal eutectic grains. The effect on the VNIR spectral region was to change the magnitude but not the spectra features observed. The same result was observed by Friedlander et al. (2015), who also report increases in site disorder with shock pressure and varying effects depending on site occupancy. As such, it is difficult to generalize the effects of shock on meteorite spectra. But it is also reasonable to expect that asteroid surfaces themselves will show evidence of shock. In this sense, our terrestrial suites of meteorites may be excellent analogs for asteroid surfaces, especially for parent bodies of ordinary, enstatites, carbonaceous chondrites, basaltic achondrites and ureilites (Bischoff and Stöffler, 1992), in which varying stages of shock metamorphism are observed.

5.3.3. Effects of weathering on classification

Weathering is known to have an effect on both meteorite (from interactions with terrestrial conditions) and asteroid spectra (from space weathering). For example, terrestrial weathering of meteorites causes a concave shoulder absorption around 0.5 μm due mostly to iron hydroxides and a band at 0.9 μm, often overlapped with a pyroxene band (Takahiro Hiroi, personal communication, 2021). In contrast, space weathering tends to change any shape into a smoother, slightly convex shape (Hiroi et al., 2006). However, variations in this small, mostly-UV region of the affected wavelengths will only affect a few input features,

and thus should not influence the overall shapes of the curves that form the basis for the algorithms. This is borne out by the concurrence between the new meteorite-based classifier and prior asteroid-based Bus-DeMeo classifier, which suggests that terrestrial weathering effects do not overly influence asteroid classification outcomes. In other words, features arising from primary mineralogy (e.g., phases with abundances greater than ~5% such as glass, olivine, and pyroxene) have a far greater effect on spectral shape than minor variations due to weathering.

Weathering may also lead to albedo variations, which should be removed by normalization. Slope differences will not greatly change the "peaks" and valleys" in the data, which are the main features that are found by the ML algorithms. In other words, the overall shape of the features from the mineral phases present is used by the algorithms, not those subtle variations. This allows the classifiers to "see through" the albedo and slope differences. Finally, models used for this study are regularized LR and SVMs with only 30 features and over a thousand training samples. This situation is not prone to overfitting (Hastie et al., 2009). Therefore models should be robust to small changes in input features such as those induced by weathering.

5.3.4. Other considerations

Any asteroid classification will be limited by the spatial scale of observations relative to the heterogeneity of the asteroid's surface. For example, DellaGiustina et al. (2020) showed that asteroid Bennu, which is a primitive body, has exogenic basaltic boulders on its surface. However, the abundances of these basaltic boulders are much too small to noticeably affect Earth-based telescopic spectra of Bennu. These scenarios cannot be easily modeled by *any* classification based on remote observations that sample at large scales, and will lead to classification based on the mixture of the exogenic material with that of the surface if the exogenic material has a high enough abundance to affect the spectral properties of the asteroid.

Phase angle effects are discussed at length in Binzel et al. (2019). They compare multiple observation of several NEAs ((433) Eros, (1036) Ganymede, (1627) Ivar, and (4179) Toutatis) and conclude that "there is no single phase correction that is applicable to all objects; the value may be dependent on the individual object." For that reason, they employ only spectra of objects as measured. This study follows that precedent. However, we note that the phase angle used at RELAB to obtain the meteorite spectra in this study is 30°, which is approximately in the middle of the range for the NEAs (10 to 50°). Phase angles for the observed main belt asteroids would tend to be smaller, but the 30° angle used for the meteorite measurements would be likely to be comparable.

Binzel et al. (2019) also raise the issue of the effects of thermal tails. They result when really dark objects in the NEA population are hot enough so that their long wavelength part of their spectrum can be noticeably affected by their blackbody curve. Binzel et al. (2019) model this effect and apply their thermal correction to the NEA data that were in turn used in this study.

5.4. Relationship between asteroid composition and location

A different approach to validating the results of our meteorite-

trained classifiers is to consider whether the spatial distribution of groups makes sense in the context of what is known about Solar System formation. Fig. 7 shows the average albedo and semi-major axis lengths (excluding Mars-crossing and near-Earth objects) for asteroids in each classification.

Albedo is expected to vary with the Fe content of the various objects. HEDs should have the highest albedo because their mineralogies are dominated by Fe-free plagioclase. For example, diogenites contain most Mg-rich (rather than Fe-rich) orthopyroxenes, with small amounts of olivine and plagioclases, and their light color imparts a high albedo. The CK/BRAC-class asteroids contain high amounts of Fe-poor (Mg-rich) olivine, causing them to appear brighter. In the middle range of albedos, the metal contents of acapulcoites and lodranites reduce their albedos.

At the other end of the albedo range are EH/EL and ordinary chondrites, which tend to contain higher-Fe enstatite and more opaque phases, either in silicates or as iron metal. CO/CV objects should also be relatively dark because they are mainly opaque phases. The IAB/IIAB iron class here, also with low albedos, likely includes D-type asteroids, which tend to be organic-rich and as dark as irons. Finally, asteroids that are classified as aubrites/featureless tend to be relatively dark, which implies that are most similar to carbonaceous chondrites and not aubrites.

To evaluate the spatial distribution of the classified asteroids, the average semi-major axis for each object is shown in order of length (Fig. 7). The abundances of different asteroid types are known to vary with distance from the Sun (Gradie and Tedesco, 1982; DeMeo and Carry, 2014). Near-Earth asteroids and those crossing Mars are removed

from this data set, because their orbits have likely been perturbed. This graphic highlights a potential limitation of the current classification, which is that the relatively featureless and red spectra of the iron (IAB/IIAB) asteroid classes should be quite similar to those of the organic-rich and also featureless D-type asteroids found in the outer part of the asteroid belt. The elevated average semi-major axis lengths of the IAB/IIAB class strongly suggests that this class has ample representation from D-type asteroids, which are unfortunately not represented in our spectral library because that material has trouble surviving passage through the Earth's atmosphere. For example, asteroid (279) Thule is a D-type at ~4 AU that is classified as IAB/IIAB. Thus the IAB/IIAB class should probably be considered as the IAB/IIAB/D class. This serves as a reminder that any classification is only as good as the input (training) data.

6. Implications and future work

There are effectively three approaches to understanding asteroid provenance. The first utilizes the approaches laid out in the Asteroids IV volume (e.g., Reddy et al., 2015), in which understanding asteroid composition depends on comparisons to laboratory measurements of mafic minerals, which reveal characteristics of olivine and pyroxene minerals that occur in many types of meteorites and asteroids. The second (used here) uses meteorite spectra without assumptions about mineralogy, but simply as representatives of their types, and builds a classifier that is then directly applied to asteroids. The third classifies asteroids based solely on other asteroid spectra, without regard for their meteorite analogs. Each approach has advantages and disadvantages, and ultimately, the best taxonomy may arise from some combination of them.

Recent work by DeMeo et al. (2022) moves in this direction by summarizing spectral similarities between meteorites and asteroids using spectral features (e.g., absorption bands and curvature of spectra). They find connections between ordinary chondrites and S-complex and Q-type asteroids; pristine CM carbonaceous chondrites with Ch-type asteroids; heated CMs with C-type asteroids; HED meteorites with V-types; enstatite chondrites with Xc-type asteroids; CV chondrites with K-type asteroids; and brachinites, pallasites, and R chondrites with olivine dominated A-type asteroids. Many of these associations are seen in our data. We find that our H/L/LL/ureilite group tends to match with S-complex and Q-type bodies, our V-type group with HEDs, our Xc group (and Xe group) tends to match with enstatite chondrites.

The planetary science community has become accustomed to the current BDM paradigm for asteroid taxonomy, which was pioneering for its time. In recent years, as aptly noted by Penttilä et al. (2021), there is currently a burgeoning of possible classification techniques, with novel techniques applied following each latest introduction of additional asteroid data. Most use unlabeled classifications or those based on labels from the Bus-DeMeo system (see Section 5.3 above). This paper proposes a fundamentally different approach to the problem because it is based on the existing meteorite classification system, which is based on known compositions and mineralogies. Thus, the classifier proposed here is firmly grounded in physical knowledge of the training samples.

Three lines of evidence support the usefulness of the proposed new classifier. Models concur in predicting an appropriate composition based on other knowledge of those objects, the results are mostly consistent with the existing Bus-DeMeo classification, and the predicted asteroid groups make sense in terms of our understanding of the distribution of material in the Solar System. Moreover the proposed classification system is fully automatic and does not require any human interaction for classification. The groups are rooted in mineralogy, providing a deeper understanding of the potential mineralogical compositions of asteroids. The proposed classification uses the shape of the spectra and is not dependent on minor variations such as those introduced by terrestrial (on the meteorites) or space (on the asteroid) weathering. Finally, it relates meteorites to their potential parent bodies.
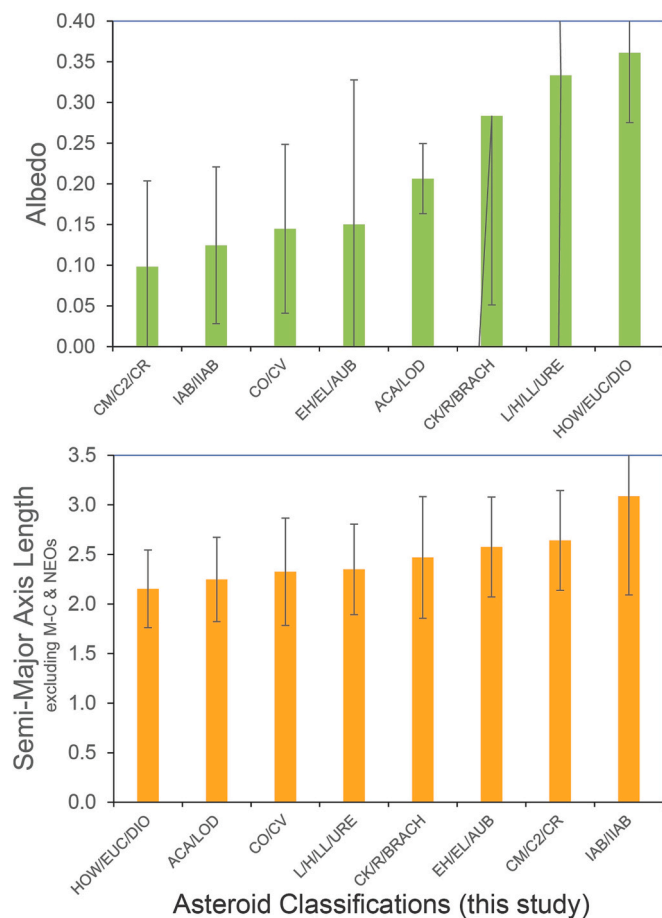

Fig. 7. Ranked albedo and semi-major axes lengths of classes predicted by this study. Average and standard deviation (represented by error bars) values of albedo and semi-major axis lengths (excluding Mars-crossing and near-Earth objects) in the new classification.

Looking to the future, machine learning methods are sure to improve, but a fundamental limitation of this approach remains the paucity of spectroscopic data on different meteorite types, especially specific groups such as acapulcoites and CB chondrites. As new meteorites are found and those spectral libraries grow, this analysis can easily be redone to update it. This paper lays a firm foundation on which subsequent taxonomic studies can build.

Declaration of Competing Interest

Data availability

RELAB meteorite data are given in Excel table Data S1. Meteorite data from the University of Winnipeg are in Excel table Data S2. Asteroid spectra used herein given in Excel table Data S3.

Acknowledgments

Appendix A. Supplementary data

Supplementary data to this article can be found online at https://doi.org/10.1016/j.icarus.2023.115718.

References

Adams, J.B., Hörz, F., Gibbons, R.V., 1979. Effects of shock-loading on the reflectance spectra of plagioclase, pyroxene, and glass. In: Proc. Lunar and Planet. Sci. Conf. 10th. Lunar and Planetary Institute, Houston, Tex, pp. 5–7.

Bell, J.F., 1989. Asteroids II. University of Arizona Press, pp. 921–944.

Binzel, R.P., DeMeo, F.E., Turtelboom, E.V., Bus, S.J., Tokunaga, A., Burbine, T.H., Lantz, C., Polishook, D., Carry, B., Morbidelli, A., Birlan, M., Vernazza, P., Burt, B.J., Moskovitz, N., Slivan, S.M., Thomas, C.A., Rivkin, A.S., Hicks, M.D., Dunn, T., Reddy, V., Sanchez, J.A., Granvik, M., Kohout, T., 2019. Compositional distributions and evolutionary processes for the near-Earth object population: results from the MIT-Hawaii Near-Earth Object Spectroscopic Survey (MITHNEOS). Icarus 324, 41–76. https://doi.org/10.1016/j.icarus.2018.12.035.

Bischoff, A., Stöffler, D., 1992. Shock metamorphism as a fundamental process in the evolution of planetary bodies: information from meteorites. Eur. J. Mineral. 4 (4), 707–755. https://doi.org/10.1127/ejm/4/4/0707.

Bruckenthal, E.A., Pieters, C.M., 1984. Spectral effects of natural shock on plagioclase feldspar. In: Proceedings of the 15th Lunar and Planetary Science Conference. Lunar and Planetary Institute, Houston, TX, pp. 96–97.

Burbine, T.H., 1998. Could G-class asteroids be the parent bodies of the CM chondrites? Meteor. Planet. Sci. 33, 253–258. https://doi.org/10.1111/j.1945-5100.1998.tb01630.x.

Burbine, T.H., 2017. Asteroids: astronomical and geological bodies. Cambridge University Press.

Burbine, T.H., Wallace, S.M., Dyar, M.D., 2019. Applying the Bus-DeMeo asteroid taxonomy to meteorite spectra. In: LPSC 50, #1655.

Bus, S.J., Binzel, R.P., 2002a. Phase I of the small main-belt asteroid spectroscopic survey: a feature-based taxonomy. Icarus 158, 146–177. https://doi.org/10.1006/icar.2002.6856.

Bus, S.J., Binzel, R.P., 2002b. Phase II of the small main-belt asteroid spectroscopic survey: the observations. Icarus 158, 106–145. https://doi.org/10.1006/icar.2002.6857.

Carey, C., Dyar, M.D., Boucher, T., Giguere, S., 2017. Web-based software for preprocessing, matching, fitting, prediction and visualization of spectroscopic data: the data exploration, visualization, and analysis of spectra (DEVAS) website. Lunar Planet. Sci. Conf. Abstr. 48, 1097.

Chapman, C.R., 1996. S-type asteroids, ordinary chondrites, and space weathering: the evidence from Galileo's fly-bys of Gaspra and Ida. Meteor. Planet. Sci. 31, 699–725. https://doi.org/10.1111/j.1945-5100.1996.tb02107.x.

Chapman, C.R., Morrison, D., Zellner, M., 1975. Surface properties of asteroids: a synthesis of polarimetry, radiometry, and spectrophotometry. Icarus 25, 104–130. https://doi.org/10.1016/0019-1035(75)90191-8.

Clark, B.E., Bus, S.J., Rivkin, A.S., McConnochie, T., Sanders, J., Shah, S., Hiroi, T., Shepard, M., 2004. E-type asteroid spectroscopy and compositional modeling. J. Geophys. Res. Planets 109, E02001. https://doi.org/10.1029/2003JE002200.

Clark, B.E., Ziffer, J., Nesvorny, D., Campins, H., Rivkin, A.S., Hiroi, T., Barucci, M.A., Fulchignoni, M., Binzel, R.P., Fornasier, S., DeMeo, F., Ockert-Bell, M.E., Licandro, J., Mothé-Diniz, T., 2010. Spectroscopy of B-type asteroids: subgroups and meteorite analogs. JGR Planets 115, E06005. https://doi.org/10.1029/2009JE003478.

Cobas, J.C., Bernstein, M.A., Martin-Pastor, M., Garcia-Tahoces, P., 2006. A new general-purpose fully automatic baseline-correction procedure for 1D and 2D NMR data. J. Magn. Res. 183 https://doi.org/10.1016/j.jmr.2006.07.013, 145–15.

Colazo, M., Alvarez-Candal, A., Duffard, R., 2022. Zero-phase angle asteroid taxonomy classification using unsupervised machine learning algorithms. Astron. Astrophys. 666, A77. https://doi.org/10.1051/0004-6361/202243428.

DellaGiustina, D.N., Burke, K.N., Walsh, K.J., Smith, P.H., Golish, D.R., Bierhaus, E.B., Ballouz, R.L., Becker, T.L., Campins, H., Tatsumi, E., Yumoto, K., Sugita, S., Deshapriya, J.D.P., Cloutis, E.A., Clark, B.E., Hendrix, A.R., Sen, A., Al Asad, M.M., Daly, M.G., Applin, D.M., Avdellidou, C., Barucci, M.A., Becker, K.J., Bennett, C.A., Bottke, W.F., Brodbeck, J.I., Connolly Jr., H.C., Delbo, M., de Leon, J., Drouet d`Aubigny, C.Y., Edmundson, K.L., Fornasier, S., Hamilton, V.E., Hasselmann, P.H., Hergenrother, C.W., Howell, E.S., Jawin, E.R., Kaplan, H.H., Le Corre, L., Lim, L.F., Li, J.Y., Michel, P., Molaro, J.L., Nolan, M.C., Nolau, J., Pajola, M., Parkinson, A., Popescu, M., Porter, N.A., Rizk, B., Rizos, J.L., Ryan, A.J., Rozitis, B., Shultz, N.K., Simon, A.A., Trang, D., Van Auken, R.B., Wolner, C.W.V., Lauretta, D.S., 2020. Variations in color and reflectance on the surface of asteroid (101955) Bennu. Science 370 (6517), eabc3660. https://doi.org/10.1126/science.abc3660.

DeMeo, F.E., Carry, B., 2014. Solar system evolution from compositional mapping of the asteroid belt. Nature 505, 629–634. https://doi.org/10.1038/nature12908.

DeMeo, F.E., Binzel, R.P., Slivan, S.M., Bus, S.J., 2009. An extension of the Bus asteroid taxonomy into the near-infrared. Icarus 202, 160–180. https://doi.org/10.1016/j.icarus.2009.02.005.

DeMeo, F.E., Burt, B.J., Marsset, M., Polishook, D., Burbine, T.H., Carry, B., Binzel, R.P., Vernazza, P., Reddy, V., Tang, M., Thomas, C.A., Rivkin, A.S., Moskovitz, N.A., Slivan, S.M., Bus, S.J., 2022. Connecting asteroids and meteorites with visible and near-infrared spectroscopy. Icarus 380, 114971. https://doi.org/10.1016/j.icarus.2022.114971.

Eilers, P.H.C., Boelens, H.F.M., 2005. Baseline correction with asymmetric least squares smoothing. In: Leiden University Medical Centre Report.

Elkins-Tanton, L.T., Asphaug, E., Bell III, J.F., Bercovici, H., Bills, B., Binzel, R., Bottke, W.F., Dibb, S., Lawrence, D.J., Marchi, S., McCoy, T.J., Oran, R., Park, R.S., Peplowski, P.N., Polanskey, C.A., Prettyman, T.H., Russell, C.T., Schaefer, L., Weiss, B. P., Wieczorek, M.A., Williams, D.A., Zuber, M.T., 2020. Observations, meteorites, and models: a preflight assessment of the composition and formation of (16) Psyche. J. Geophys. Res. Planets 125. https://doi.org/10.1029/2019JE006296 e2019E006296.

Friedlander, L.R., Glotch, T.D., Bish, D.L., Dyar, M.D., Sharp, T.G., Sklute, E.C., Michalski, J.R., 2015. Structural and spectroscopic changes to natural nontronite induced by experimental impacts between 10 and 40 GPa. JGR Planets 120, 888–912. https://doi.org/10.1002/2014JE004638.

Gaffey, M.J., Gilbert, S.L., 1998. Asteroid 6 Hebe: the probable parent body of the H-type ordinary chondrites and the IIE iron meteorites. Meteor. Planet. Sci. 33, 1281–1295. https://doi.org/10.1111/j.1945-5100.1998.tb01312.x.

Gradie, J., Tedesco, E., 1982. Compositional structure of the asteroid belt. Science 216, 1405–1407. https://doi.org/10.1126/science.216.4553.14.

Granvik, M., Brown, P., 2018. Identification of meteorite source regions in the Solar System. Icarus 311, 271–287. https://doi.org/10.1016/j.icarus.2018.04.012.

Hastie, T., Tibshirani, R., Friedman, J.H., Friedman, J.H., 2009. The Elements of Statistical Learning: Data Mining, Inference, and Prediction (2). Springer, New York, pp. 1–758. https://hastie.su.domains/ElemStatLearn/.

Hiroi, T., Abe, M., Kitazato, K., Abe, S., Clark, B.E., Sasaki, S., Ishiguro, M., Barnouin-Jha, O.S., 2006. Developing space weathering on the asteroid 25143 Itokawa. Nature 443, 56–58. https://doi.org/10.1038/nature05073.

Johnson, J.R., Hörz, F., 2003. Visible/near-infrared spectra of experimentally shocked plagioclase feldspars. J. Geophys. Res. 108 (E11), 5120. https://doi.org/10.1029/2003JE002127.

Kajfosz, J., Kwiatek, W.M., 1987. Nonpolynomial approximation of background in X-ray spectra. Nucl. Instr. Methods Phys. Res. 22, 78–81. https://doi.org/10.1016/0168-583X(87)90298-9.

Kargel, J.S., 1994. Metalliferous asteroids as potential sources of precious metals. J. Geophys. Res. Planets 99, 21129–21141. https://doi.org/10.1029/94JE02141.

Klimczak, H., Kotlowski, M., Oszkiewicz, D., DeMeo, F., Kryszczuńska, A., Wilawer, E., Carry, B., 2021. Predicting asteroid types: importance of individual and combined features. Front. Astron. Space Sci. 8, 767885 https://doi.org/10.3389/fspas.2021.767885.

Klimczak, H., Oszkiewicz, D., Carry, B., Pentillä, A., Kotlowski, W., Kryszczuńska, A., Wilawer, E., 2022. Comparison of machine learning algorithms used to classify the asteroids observed by all-sky surveys. Astron. Astrophys. 667, A10. https://doi.org/10.1051/0004-6361/202243889.

Kohout, T., Petrova, E.V., Yakovlev, G.A., Grokhovsky, V.I., Penttilä Maturillia, A., Moreau, J.G., Berzin, S.V., Wasiljeff, J., Danilenko, I.A., Zamyatin, D.A.,

Muftakhetdinova, R.F., Heikkila, M., 2020. Experimental constraints on the ordinary chondrite shock darkening caused by asteroid collisions. Astron. Astrophys. 639, A146. https://doi.org/10.1051/0004-6361/202037593.

Korda, D., Penttilä, A., Klami, A., Kohout, T., 2023. Neural network for determining an asteroid mineral composition from reflectance spectra. Astron. Astrophys. 669, A101. https://doi.org/10.1051/0004-6361/202243886.

Larson, H.P., Fink, U., 1975. Infrared spectral observations of asteroid 4 Vesta. Icarus 26 (4), 420–427. https://doi.org/10.1016/0019-1035(75)90109-8.

Lauretta, D.S., Balram-Knutson, S.S., Beshore, E., Boynton, W.V., d'Aubigny, C.D., DellaGiustina, D.N., Enos, H.L., Goklish, D.R., Hergenrother, C.W., Howell, E.S., Bennett, C.A., Morton, E.T., Nolan, M.C., Rizk, B., Roper, H.L., Bartels, A.E., Bos, B. J., Dworkin, J.P., Highsmith, D.E., Lorenz, D.A., Lim, L.F., Mink, R., Moreau, M.C., Nuth, J.A., Reuther, D.C., Simon, A.A., Bierhaus, E.B., Bryan, B.H., Ballouz, R., Barnouin, O.S., Binzel, R.P., Bottke, W.F., Hamilton, V.E., Walsh, K.J., Chesley, S.R., Christensen, P.R., Clark, B.E., Connolly, H.C., Crombie, D.J., Daly, M.G., Energy, J. P., McCoy, T.J., McMahon, J.W., Scheeres, D.J., Messenger, S., Nakamura-Messenger, K., Righter, K., Sandford, S.A., 2017. OSIRIS-REx: sample return from asteroid (101955) Bennu. Space Sci. Rev. 212, 925–984. https://doi.org/10.1007/s11214-017-0405-1.

Levinson, H.F., Olkin, C.B., Noll, K.S., Marchi, S., Bell, J., Bierhaus, E., Binzel, R., Bottke, W., Britt, D., Brown, M., Buie, M., Christensen, P., Emery, J., Grundy, W., Hamilton, V.E., Howett, C., Mottola, S., Patzold, M., Reuter, D., Spencer, J., Statler, T.S., Stern, S.A., Sunshine, J., Weaver, H., Wong, I., 2021. Lucy mission to the Trojan asteroids: science goals. Planet. Sci. J. 2, 171. https://doi.org/10.3847/PSJ/abf840.

Li, Z., Zhan, D.J., Wang, J.J., Huang, J., Xu, Q.S., Zhang, Z.M., Zheng, Y.B., Liang, Y.Z., Wang, H., 2013. Morphological weighted penalized least squares for background correction. Analyst 138, 4483–4492. https://doi.org/10.1039/C3AN00743J.

Mahlke, M., Carry, B., Mattei, P.-A., 2022. Asteroid taxonomy from cluster analysis of spectrometry and albedo. Astron. Astrophys. 665, A26. https://doi.org/10.1051/0004-6361/202243587.

Matter, A., Delbo, M., Carry, B., Ligori, S., 2013. Evidence of a metal-rich surface for the Asteroid (16) Psyche from interferometric observations in the thermal infrared. Icarus 226, 419–427. https://doi.org/10.1016/j.icarus.2013.06.004.

McCord, T.B., Adams, J.B., Johnson, T.V., 1970. Asteroid Vesta: spectral reflectivity and compositional implications. Science 168, 1445–1447. https://doi.org/10.1126/science.168.3938.1445.

McCoy, T.J., Keil, K., Clayton, R.N., Mayeda, T.K., Bogard, D.D., Garrison, D.H., Wiel, R., 1997. A petrologic and isotopic study of lodranites: evidence for early formation as partial melt residues from heterogeneous precursors. Geochim. Cosmochim. Acta 61, 623–637. https://doi.org/10.1016/S0016-7037(96)00359-6.

McSween Jr., H.Y., Binzel, R.P., De Sanctis, M.C., Ammannito, E., Prettyman, T.H., Beck, A.W., Reddy, V., Le Corre, L., Gaffey, M.J., McCord, T.B., Raymond, C.A., Russell, C.T., Dawn Science Team, 2013. Dawn; the Vesta-HED connection; and the geologic context for eucrites, diogenites, and howardites. Meteor. Planet. Sci. 48, 2090–2104. https://doi.org/10.1111/maps.12108.

Mika, S., Rätsch, G., Müller, K., 2001. A mathematical programming approach to the Kernel Fisher algorithm. In: Jai, M. (Ed.), Neural Information Processing Systems, vol. 13. MIT Press, pp. 591–597.

Nakamura, T., Noguchi, T., Tanaka, M., Zolensky, M.E., Kimura, M., Tsuchiyama, A., Nakato, A., Ogami, T., Ishida, H., Uesugi, M., Yada, T., Shirai, K., Fujimura, A., Okazaki, R., Sandford, S.A., Ishibashi, Y., Abe, M., Okada, T., Ueno, M., Mukai, T., Yoshikawa, M., Kawaguchi, J., 2011. Itokawa dust particles: a direct link netween S-

type asteroids and ordinary ohondrites. Science 333, 1113–1115. https://doi.org/10.1126/science.1207758.

Oszkiewicz, D.A., Kwiatkowski, T., Tomov, T., Birlan, M., Geier, S., Penttilä, A., Polińska, M., 2014. Selecting asteroids for a targeted spectroscopic survey. Astron. Astrophys. 572, A29. https://doi.org/10.1051/0004-6361/201323250.

Oszkiewicz, D., Troiansky, V., Galád, A., Hanuš Ďurech, J., Wilawer, E., Marciniak, A., Kwiatkowski, T., Koleńczuk, P., Skiff, B.A., Polakis, T., Moskovitz, N.A., Geier, S., Föhring, D., Hung, D., Gajdoš, Š., Világi, J., Polčic, L., Kushuba, V., Udovichenko, S., Keir, L., Benishek, V., Pray, D.P., Shevchenko, V., Krugly, Y., Kankiewicz, P., Hasegawa, S., Behrend, R., Bernasconi, L., Leroy, A., Roy, R., Ivanova, O., Husárik, M., DSimon, A., 2023. Spins and shapes of basaltic asteroids and the missing mantle problem. Icarus 397, 115520. https://doi.org/10.1016/j.icarus.2023.115520.

Penttilä, A., Hietala, H., Muinonen, K., 2021. Asteroid spectral taxonomy using neural networks. Astron. Astrophys. 649, A46. https://doi.org/10.1051/0004-6361/202038545.

Penttilä, A., Fedorets, G., Muinonen, K., 2022. Taxonomy of asteroids from the Legacy Survey of space and time using neural networks. Front. Astron. Space Sci. 9, 816268 https://doi.org/10.3389/fspas.2022.816268.

Popescu, M., Birlan, M., Nedelcu, D.A., 2012. Modeling of asteroid spectra – M4AST. Astron. Astrophys. 544, A130. https://doi.org/10.1051/0004-6361/201219584.

Reddy, V., Dunn, T.L., Thomas, C.A., Moskovitz, N.A., Burbine, T.H., 2015. Mineralogy and surface composition of asteroids. In: Michel, P., DeMeo, F.E., Bottke, W.F. (Eds.), Asteroids IV, pp. 43–63.

Reddy, V., Sanchez, J.A., Furfaro, R., Binzel, R.P., Burbine, T.H., Le Corre, L., Hardersen, P.S., Bottke, W.F., Brozovic, M., 2018. Surface composition of (99942) Apophis. Astron. J. 155, 140. https://doi.org/10.3847/1538-3881/aaaa1c.

Roberts, S., Sheffer, A., Dyar, M.D., McCanta, M., Sklute, E.C., 2019. Oxidation state of iron in fulgurites and trinitite: implications for redox changes during abrupt high-temperature and pressure events. Geochim. Cosmochim. Acta 266, 332–350.

Russell, C.T., Raymond, C.A., 2011. The Dawn mission to Vesta and Ceres. Space Sci. Rev. 163, 3–23. https://doi.org/10.1007/s11214-011-9836-2.

Scott, E.R.D., Greenwood, R.C., Franchi, I.A., Sanders, I.S., 2009. Oxygen isotopic constraints on the origin and parent bodies of eucrites, diogenites, and howardites. Geochim. Cosmochim. Acta 73, 5835–5853. https://doi.org/10.1016/j.gca.2009.06.024.

Tholen, D.J., 1984. Asteroid Taxonomy from Cluster Analysis of Photometry. PhD Thesis,. University of Arizona, p. 166.

Treiman, A.H., Dyar, M.D., McCanta, M., Noble, S.K., Pieters, C.M., 2007. Martian dunite NWA 2737: petrographic constraints on geological history, shock events, and olivine color. JGR (Planets) 112, E04002. https://doi.org/10.1029/2006JE002777.

Vernazza, P., Binzel, R.P., Thomas, C.A., DeMeo, F.E., Bus, S.J., Rivkin, A.S.m., Tokunaga, A.T., 2008. Compositional differences between meteorites and near-Earth asteroids. Nature 454 (7206), 858–860. https://doi.org/10.1038/nature07154.

Yada, T., Abe, M., Okada, T., et al., 2022. Preliminary analysis of the Hayabusa2 samples returned from C-type asteroid Ryugu. Nat. Astron. 6, 214–220. https://doi.org/10.1038/s41550-021-01550-6.

Zellner, B., Thirunagari, A., Bender, D., 1985. The large-scale structure of the asteroid belt. Icarus 62, 505–511. https://doi.org/10.1016/0019-1035(85)90190-3.

Zhang, Z.-M., Chen, S., Liang, Y.Z., 2010. Baseline correction using adaptive iteratively reweighted penalized least squares. Analyst 135, 1138–1146. https://doi.org/10.1039/B922045C.